



Original article

Inhibition of histone methyltransferase PRMT5 attenuates cisplatin-induced hearing loss through the PI3K/Akt-mediated mitochondrial apoptotic pathway

Zhiwei Zheng^{a,1}, Benyu Nan^{b,1}, Chang Liu^{c,1}, Dongmei Tang^a, Wen Li^a, Liping Zhao^a, Guohui Nie^{d,**}, Yingzi He^{a,*}

^a ENT Institute and Department of Otorhinolaryngology, Eye & ENT Hospital, State Key Laboratory of Medical Neurobiology and MOE Frontiers Center for Brain Science, NHC Key Laboratory of Hearing Medicine (Fudan University), Fudan University, Shanghai, 200031, China

^b Department of Otorhinolaryngology-Head and Neck Surgery, The Second Affiliated Hospital and Yuying Children's Hospital of Wenzhou Medical University, Wenzhou, 325000, Zhejiang, China

^c Department of Otolaryngology-Head and Neck Surgery, The Third Affiliated Hospital of Sun Yat-Sen University, Guangzhou, 510630, China

^d Department of Otolaryngology, Shenzhen Institute of Translational Medicine, Shenzhen Second People's Hospital, The First Affiliated Hospital of Shenzhen University, Shenzhen, 518035, Guangdong, China

ARTICLE INFO

Article history:

Received 22 December 2022

Received in revised form

19 April 2023

Accepted 21 April 2023

Available online 26 April 2023

Keywords:

Protein arginine methyltransferase 5

(PRMT5)

LLY-283

Cisplatin

Hearing loss

Hair cell

Spiral ganglion neuron

ABSTRACT

This study aimed to evaluate the therapeutic potential of inhibiting protein arginine methyltransferase 5 (PRMT5) in cisplatin-induced hearing loss. The effects of PRMT5 inhibition on cisplatin-induced auditory injury were determined using immunohistochemistry, apoptosis assays, and auditory brainstem response. The mechanism of PRMT5 inhibition on hair cell survival was assessed using RNA-seq and Cleavage Under Targets and Tagment-quantitative polymerase chain reaction (CUT&Tag-qPCR) analyses in the HEI-OC1 cell line. Pharmacological inhibition of PRMT5 significantly alleviated cisplatin-induced damage to hair cells and spiral ganglion neurons in the cochlea and decreased apoptosis by protecting mitochondrial function and preventing the accumulation of reactive oxygen species. CUT&Tag-qPCR analysis demonstrated that inhibition of PRMT5 in HEI-OC1 cells reduced the accumulation of H4R3me2s/H3R8me2s marks at the promoter region of the *Pik3ca* gene, thus activating the expression of *Pik3ca*. These findings suggest that PRMT5 inhibitors have strong potential as agents against cisplatin-induced ototoxicity and can lay the foundation for further research on treatment strategies of hearing loss.

© 2023 The Authors. Published by Elsevier B.V. on behalf of Xi'an Jiaotong University. This is an open access article under the CC BY-NC-ND license (<http://creativecommons.org/licenses/by-nc-nd/4.0/>).

1. Introduction

Hearing loss caused by damage to cochlear hair cells (HCs) or spiral ganglion neurons (SGNs) is a common side-effect for patients treated with various ototoxic insults, thereby often resulting in irreversible, accumulative, bilateral, and sensorineural hearing loss. Currently, many otoprotective agents are being investigated, and various types of protectants have been identified in animal studies for preventing deafness induced by cisplatin, carboplatin,

aminoglycoside, or noise exposure. In recent years, epigenetic modifications, particularly those catalyzed by histone-modifying enzymes, have been shown to play a crucial role in inner ear morphogenesis and HC differentiation [1–7]. These modifications regulate HC survival [8] and are associated with the induction of sensorineural hearing loss [9,10]. Epigenetic modifications are posttranslational modifications (PTM), and thus do not alter the intrinsic DNA sequence or structure [11–13]. Therefore, epigenetic regulators and associated mechanisms might provide a perfect strategy for managing ototoxic insult-induced auditory damage.

Arginine methylation, which is catalyzed by protein arginine methyltransferases (PRMTs), is a frequently occurring post-translational modification (PTM) involved in transcriptional activation and repression [14]. PRMTs are divided into type I and type II enzymes, producing asymmetric and symmetric dimethylarginine,

Peer review under responsibility of Xi'an Jiaotong University.

* Corresponding author.

** Corresponding author.

E-mail addresses: nieguohui@email.szu.edu.cn (G. Nie), yingzihe09611@126.com (Y. He).

¹ These authors contributed equally to this work.

<https://doi.org/10.1016/j.jpha.2023.04.014>

2095-1779/© 2023 The Authors. Published by Elsevier B.V. on behalf of Xi'an Jiaotong University. This is an open access article under the CC BY-NC-ND license (<http://creativecommons.org/licenses/by-nc-nd/4.0/>).

respectively [14]. Our previous study demonstrated that protein arginine methyltransferase 6 (PRMT6) mediates ototoxic insult-induced hair cell death [15]. However, little is known about the actions of other members of the PRMT family and the mechanisms that regulate the survival of sensory HCs.

As a type II PRMT, PRMT5 induces the symmetric dimethylation of histone H3 residue arginine 8 (H3R8me2s) and H4 residue arginine 3 (H4R3me2s), thereby controlling gene transcription [16,17]. PRMT5-mediated arginine methylation has been implicated in many cellular processes, including cell growth [17,18], metastasis [19], ribosome biogenesis [20], cell differentiation [21], and gene transcription [22,23]. Interestingly, PRMT5 has been involved in the development of various human tumors, such as leukemia, glioblastoma, lymphoma, and gastric and breast cancer, making it an attractive target for the treatment of these diseases [13,24–26]. Furthermore, PRMT5 is essential for maintaining the pluripotency of both embryonic and neural stem cells [27,28], and its absence can disrupt normal hematopoiesis [29]. Additionally, PRMT5 was shown to regulate the activity of nuclear transcription factor- κ B (NF- κ B) through tumor necrosis factor (TNF)-related apoptosis-inducing ligand (TRAIL) and methylation of the p65 subunit, thereby affecting NF- κ B-dependent gene expression [30,31]. Recent studies suggested that PRMT1 and PRMT5 are activated during hypoxia- and ischemia-induced apoptosis, while inhibition of the activation of PRMT1, PRMT5, or mitogen-activated protein kinase (MAPK) (p38 and c-Jun N-terminal kinase (JNK)) can reduce apoptosis [32]. PRMT5 was also reported to be highly expressed in the renal tubular epithelium of an ischemic/reperfusion injury animal model [33]. However, the role of PRMT5 in hearing loss, particularly that induced by cisplatin, has not been investigated.

This study aimed to explore the function of PRMT5 in the survival of HCs and SGNs under cisplatin-induced stimulus and the possible mechanisms underlying this process. A better understanding of the role of PRMT5 in hearing loss could provide new therapeutic strategies for clinicians.

2. Materials and methods

2.1. Compounds, HEI-OC1 cell culture, and cochlear explants

LLY-283, EPZ015666, and LY294002 were purchased from Selleckchem (Houston, TX, USA) and diluted in dimethyl sulfoxide (DMSO). HEI-OC1 cells were cultured in high-glucose Dulbecco's modified Eagle's medium (DMEM) (Gibco BRL, Grand Island, NY, USA) supplemented with 5% fetal bovine serum (FBS; Gibco BRL) at 37 °C and 10% CO₂.

The Institutional Animal Care and Use Committee of Fudan University approved all animal experiments (Approval number: IACUC-DWZX-2023-031). Cochleae were dissected from C57BL/6J mice at postnatal day 2 (P2) and placed in phosphate buffered solution (PBS). Coverslips were flattened and coated with Cell-Tak (BD Biosciences, San Jose, CA, USA). The cochlear explants were stuck onto them and incubated at 37 °C in DMEM/F12 medium supplemented with N2/B27 (Gibco BRL) and ampicillin. All explants were maintained in a 5% CO₂ air atmosphere overnight before each experiment.

2.2. In vivo model of cisplatin-induced hearing impairment

Wild-type adult C57BL/6J mice, aged 7–8 weeks, were used for in vivo experiments. Briefly, a hearing loss model was induced by administering 30 mg/kg cisplatin (Sigma-Aldrich, St. Louis, MO, USA) via intraperitoneal (i.p.) injection. The LLY-283 treatment group received LLY-283 (10 mg/kg) via i.p. injection 2 h before cisplatin administration. To attenuate the potential kidney injury caused by cisplatin, 1 mL heated saline was injected subcutaneously twice daily

for 7 consecutive days after cisplatin administration. Following the final saline injection, mice were allowed to recover for an additional 7 days before undergoing auditory brainstem response (ABR) tests.

2.3. ABR test

The ABR test was used to measure the hearing thresholds of mice. Details of the ABR test procedure have been provided previously [34]. Briefly, mice were given i.p. anesthesia with a mixed solution of 100 mg/kg ketamine and 25 mg/kg xylazine sodium. Tucker-Davis Technology (TDT) system III (Tucker-Davis Technologies, TDT, Gainesville, FL, USA) was used for signal collection, with 5 frequencies (4 kHz, 8 kHz, 16 kHz, 24 kHz, and 32 kHz) being employed to assess the hearing threshold of mice.

2.4. Immunohistochemistry

Each cochlear was dissected into three turns (apex, middle, and base turn) and then blocked in 0.01 M PBS with 10% normal goat serum. Next, cochlear segments were incubated with primary antibodies, including anti-myosin 7a (25-6790; Proteus Biosciences, Ramona, CA, USA), anti-Tuj-1 (801202; BioLegend, San Diego, CA, USA), anti-neurofilament (ab72996; Abcam, Cambridge, UK), anti-parvalbumin (32895; Abcam), anti-cleaved caspase-3 (9664s; Cell Signaling Technology, Danvers, MA, USA), and anti-CtBP2 IgG1 (612044; BD Biosciences, Franklin Lakes, NJ, USA). After washing with PBS, samples were incubated with secondary antibodies (Invitrogen Corporation, Carlsbad, CA, USA) at 4 °C overnight. Image acquisition was performed using the TCS SP8 confocal microscope from Leica (Hamburg, Germany).

2.5. Western blotting

Total protein was extracted using the radioimmunoprecipitation assay (RIPA) lysis buffer according to the manufacturer's instructions. Equal amounts of protein samples were separated by 10% sodium dodecyl sulfate-polyacrylamide gel electrophoresis (SDS-PAGE), blotted onto polyvinylidene fluoride (PVDF) membranes, and then incubated with the following primary antibodies: anti-PRMT5 (ab109451; Abcam), anti-H4R3me2s (SAB4300870; Sigma Aldrich), anti-H3R8me2s (A-3706; Epigentek, Farmingdale, NY, USA), anti-PI3K (4249; Cell Signaling Technology, Danvers, MA, USA), anti-phosphatidylinositol 3-kinase (PI3K) (17366; Cell Signaling Technology, Inc (CST), Boston, MA, USA), anti-AKT (9272; CST), anti-p-AKT (4060; CST), and anti-glyceraldehyde 3-phosphate dehydrogenase (GAPDH). All primary antibodies were diluted to concentrations between 1:500 and 1:10,000. Membranes were then incubated with appropriate secondary antibodies for 1 h, followed by detection of protein signals using the ECL kit (Millipore, Billerica, MA, USA).

2.6. Cholecystokinin octapeptide (CCK-8) assay

To assess the viability of HEI-OC1 cells, the CCK-8 Cell Counting Kit (96992; Sigma, Saint Louis, MO, USA) was used. Briefly, cells were seeded at a density of 2×10^4 cells/mL in 96-well plates. After different treatments, the optical density (OD₄₅₀) of cultured cells in each well was monitored following the addition of the CCK-8 reagent.

2.7. Detection of reactive oxygen species (ROS)

The levels of ROS were detected using MitoSOX-Red (Molecular Probes, Eugene, OR, USA). Cochlear explants were washed several times and stained with 5 μ M MitoSOX-Red for 30 min in the dark. Images were captured using a confocal fluorescence microscope (Leica SP8, Leica, Hamburg, Germany).

2.8. RNA sequencing analysis and real-time polymerase chain reaction (PCR) quantification

Total RNA isolated from HEI-OC1 cells was used to perform RNA sequencing analysis. The RNA-Seq reads from the FASTQ files were aligned to mm10 using a standard STAR aligner and then mapped to the mouse reference genome (NCBI37). The DESeq (2012) R package was used for differential expression analysis, and the significant difference was set to P -value <0.05 , fold change >2 , and FDR <0.01 . Further, Gene Ontology (GO) enrichment and Kyoto Encyclopedia of Genes and Genomes (KEGG) pathway enrichment analyses were performed using the R package based on the hypergeometric distribution.

Total RNA was extracted from samples using the TRIzol reagent (15596018; Thermo Fisher Scientific Waltham, MA, USA). RNA concentration and purity were determined by evaluating the absorbance ratios of A260/A280 and A260/A230 using a NanoDrop 2000 Spectrophotometer (Thermo Fisher Scientific). RNA samples with values between 1.8–2.0 and 2.0–2.2 were used for subsequent analysis. cDNA was synthesized from the extracted RNA using the Transcriptor First Strand cDNA Synthesis Kit (4897030001; Roche, Indianapolis, IN, USA). Gene-specific primers that spanned intron-exon boundaries to avoid amplifying genomic DNA were designed using the Primer 5.0 software. Primer sequences are listed in Table S1. Real-time PCR was performed using SYBR Premix Ex Taq II (Takara Biomedical Technology Co., Ltd., Kusatsu, Shiga, Japan) on a quantitative real-time PCR system (CFX 96, Bio-Rad, Hercules, CA, USA). The levels of expression were normalized to that of glyceraldehyde-3-phosphate dehydrogenase (*Gapdh*) and quantified using the $2^{-\Delta\Delta CQ}$ method. To prevent contamination, strict measures were taken during all experimental processes, including using aerosol-resistant pipette tips and gloves, as well as the physical and temporal separation of nucleic acid extraction, reaction setup, and post-PCR processing. Each run included a positive control sample with a known Ct value and a negative control sample containing only nuclease-free water (no DNA). The efficiency of the PCR reaction was calculated from the slope of a standard curve generated from a serial dilution of cDNA templates.

2.9. CUT&Tag assay

CUT&Tag was performed using 1 million cells, as previously reported [35]. Primary antibodies used were anti-H4R3me2s or anti-H3R8me2s. The secondary antibody was goat anti-rabbit IgG (AS070; ABclonal, Wuhan, China) at a dilution of 1:100. Total DNA was extracted and subjected to PCR. The following primers were used to amplify the indicated region surrounding the transcription start sites of *Pik3ca*: (forward 5'-CCTCAGTTTCAGGTTCCCA-3' and reverse 5'-GCGGTTACAGAAGCAAGAAG-3'). All experiments were repeated thrice independently, and the obtained data were normalized to that of the IgG control.

2.10. HC, SGN, and presynaptic ribbon counts

The surviving HCs labeled with myosin 7a and normal nuclei were counted in 200 μm long strips at the region from base to apex. For analysis of apoptotic HCs, only the middle turn of each explant (40%–60% from the apex) was selected for quantification. SGNs were immunolabeled with an anti-Tuj-1 antibody, and all present in the middle portion of each explant were quantified. Presynaptic ribbons were stained with anti-CtBP2 antibody, and the number of CtBP2 per IHC was quantified.

2.11. Data statistics and analysis

Statistical analyses were conducted using the GraphPad Prism 8.0 software (GraphPad Software, La Jolla, CA, USA). Analysis of variance (ANOVA) analysis was performed for differentiation comparison; data were exhibited as the mean \pm standard error of the mean (SEM), and $P < 0.05$ was considered statistical significant.

3. Results

3.1. Pharmacological inhibition of PRMT5 prevented cisplatin-induced cochlear HCs loss in vitro

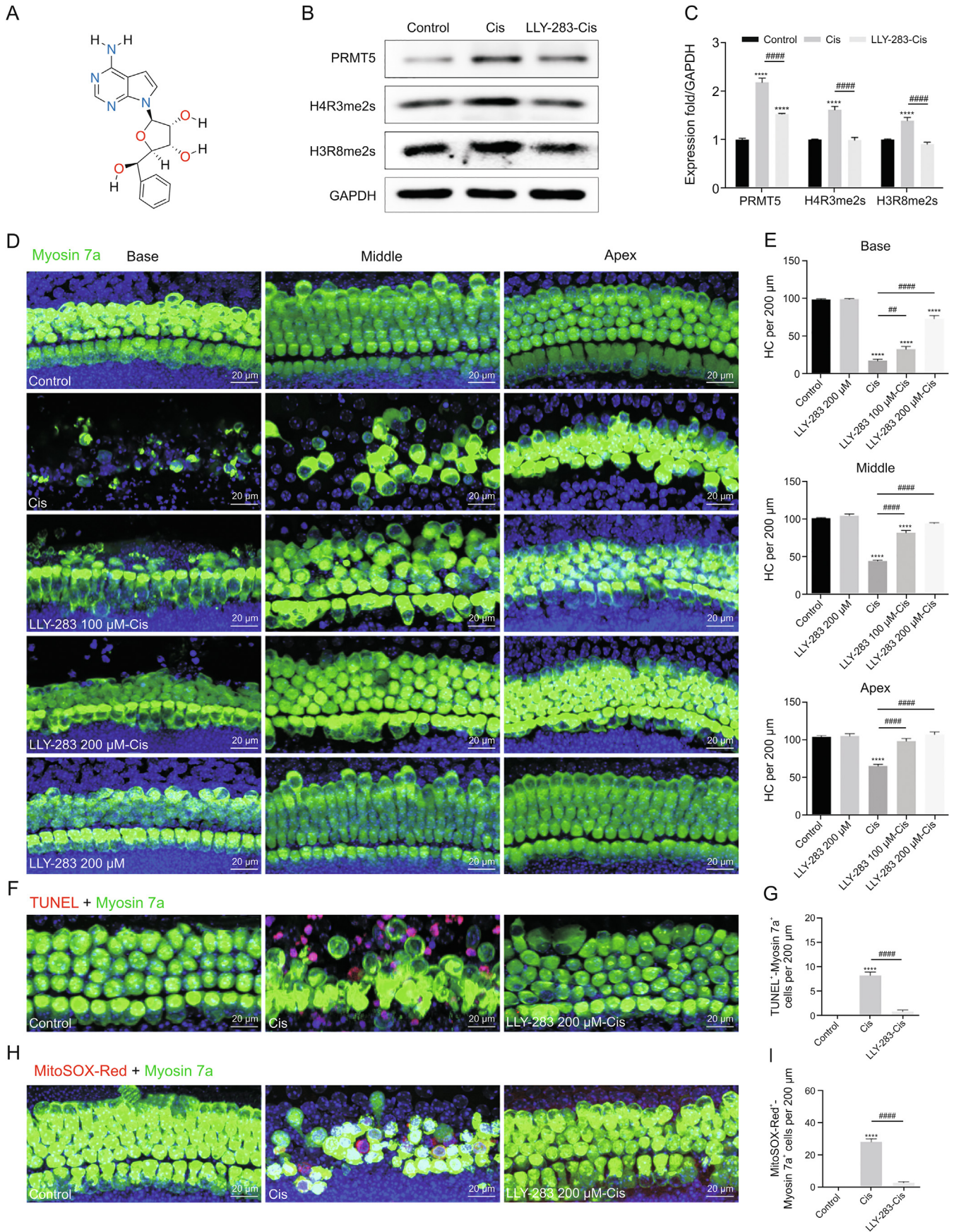
To determine the potential role of PRMT5 in cisplatin-induced ototoxicity, we first measured the expression of PRMT5 in cochlear explant cultures from P2 WT C57BL/6J mice treated with or without cisplatin by western blotting. We found that the protein level of PRMT5 was significantly increased after cisplatin treatment compared with that in the control group (Figs. 1A–C). However, pharmacological inhibition of PRMT5 using the selective and potent inhibitor LLY-283 remarkably reduced the cisplatin-induced elevation in the expression of PRMT5. To assess whether LLY-283 altered the function of PRMT5, we performed western blot analysis of symmetrical dimethyl arginine modifications catalyzed by PRMT5. We observed that the expression of symmetric H4R3me2s and H3R8me2s was significantly decreased in LLY-283-pretreated explants after cisplatin exposure compared with that in cisplatin treated explants (Figs. 1A–C).

To examine the potential protective effect of inhibiting PRMT5 on cisplatin-induced ototoxicity, we pretreated mouse cochlear explants in vitro with LLY-283 for 2 h, followed by coincubation with cisplatin for 24 h. We found that cochlear explants cultured with 20 μM cisplatin showed disarrayed HCs and severe injury, with significantly reduced numbers of HCs in the basal, middle, and apical turns (Fig. 1D). In contrast, exposure of explants to 100 or 200 μM LLY-283 for 2 h, followed by coincubation with cisplatin for another 24 h, resulted in a higher number of surviving HCs compared with that in cisplatin-treated only explants. We noticed that the best protective effect against cisplatin-induced ototoxicity was achieved with 200 μM LLY-283, which did not induce any damage to HCs. Therefore, we used 200 μM LLY-283 as the treatment dose for subsequent cochlear experiments in vitro (Fig. 1E).

To further evaluate apoptosis, we costained cochlear explants with TdT-mediated dUTP nick end labeling (TUNEL) and the hair cell-specific marker myosin 7a (Fig. 1F). Immunofluorescence staining and quantitative analysis revealed significantly lower numbers of TUNEL-labeled HCs in LLY-283-pretreated cochlear explants than in the cisplatin-treated only group (Fig. 1G). We also used MitoSOX-Red, a mitochondrial superoxide probe, to detect the levels of mitochondrial ROS (Fig. 1H). MitoSOX-Red staining of cochlear HCs showed that the levels of mitochondrial ROS were markedly reduced by LLY-283 pretreatment compared with those in cisplatin treated cochlear explants (Fig. 1I).

3.2. Inhibition of PRMT5 reduced cisplatin-induced cochlear SGN damage in vitro

To determine the effectiveness of inhibiting PRMT5 in promoting the survival of SGNs, we treated middle turn cochlear explants from P2 WT C57BL/6J mice with 20 μM cisplatin for 24 h. Representative photomicrographs of cochlear explants are shown in Figs. 2A and B. Tuj-1 staining revealed that the untreated cisplatin control group had large SGNs, with round cell bodies and projecting bursting auditory nerve fibers. However, we found that cisplatin



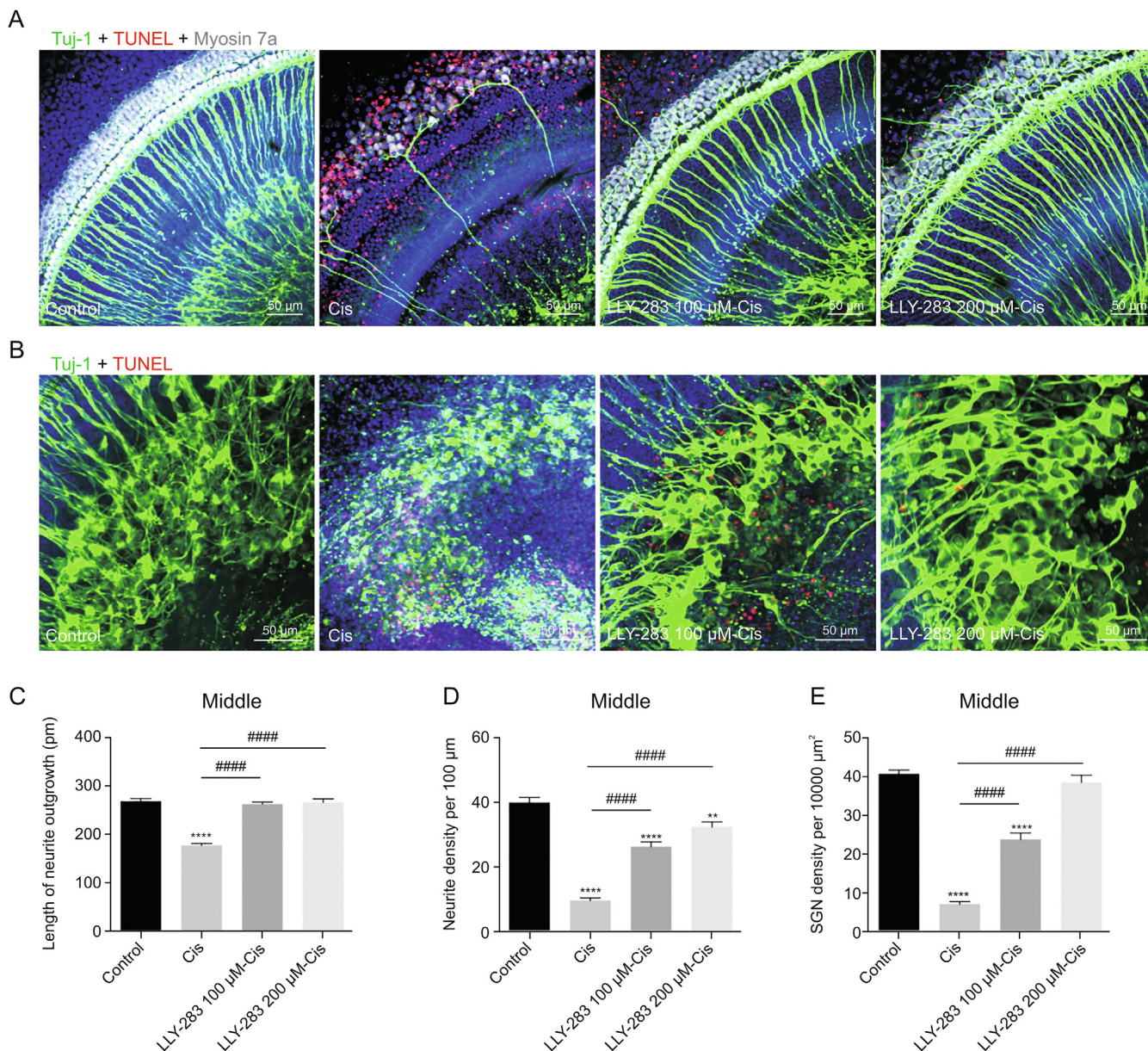


Fig. 2. LLY-283 prevents cisplatin-induced damage in SGNs in vitro. (A, B) Immunofluorescence images showing Tuj-1 (green), TUNEL (red), and myosin 7a (white) in dissected middle turns of cochleae from each treatment group. (C–E) Quantification of the length of neurite outgrowth (C), neurite densities (D), and SGN soma densities (E) from the middle turns of cochlear explants under all treatment conditions ($n = 10$ SGN explants). Data are presented as the mean \pm standard error of the mean (SEM). $^{**}P < 0.01$ and $^{****}P < 0.0001$ vs. control; $^{####}P < 0.0001$ vs. cisplatin-treated only. Cis: cisplatin; SGN: spiral ganglion neuron; TUNEL: TdT-mediated dUTP nick end labeling.

exposure significantly reduced the density of nerve fibers and SGNs compared with those in the control group. Conversely, pretreatment with LLY-283 protected nerve fibers and SGNs from cisplatin-induced damage (Figs. 2C–E). These results suggested that inhibition of PRMT5 by LLY-283 protects cultured cochlear HCs and SGNs from cisplatin-induced damage.

3.3. Pharmacological inhibition of PRMT5 reduced cisplatin-induced loss of cochlear HCs and nerves and attenuated hearing impairment in vivo

To investigate the effects of LLY-283 on cisplatin-induced hearing loss, we employed an in vivo cisplatin-injury model, as

Fig. 1. Inhibition of PRMT5 by LLY-283 prevents cisplatin-induced cochlear HCs damage in vitro. (A) Chemical structure of LLY-283. (B, C) Western blot analysis and histograms of PRMT5, H4R3me2s, and H3R8me2s. Data are presented as the mean \pm standard error of the mean (SEM). $^{****}P < 0.0001$ vs. control, $^{####}P < 0.0001$ vs. cisplatin-treated only. (D) Immunofluorescence staining with the anti-myosin 7a (green) antibody in the basal, middle, and apical turns of cochleae after different treatments. (E) Quantification of the number of myosin 7a-immunolabeled hair cells per 200 µm in the 3 turns of cochlea after different treatments ($n = 7–13$ cochleae). Data are shown as the mean \pm SEM. $^{****}P < 0.0001$ vs. control, $^{**}P < 0.01$ and $^{####}P < 0.0001$ vs. cisplatin-treated only. (F) Representative images showing immunolabeling for myosin 7a (green) and TUNEL (red) in the middle turns of cochleae. (G) Quantification of the number of TUNEL-immunolabeled hair cells per 200 µm in the middle turns of cochleae. Data are shown as the mean \pm SEM. $^{****}P < 0.0001$ vs. control, $^{####}P < 0.0001$ vs. cisplatin-treated only. (H) Representative images showing immunolabeling for MitoSOX-Red (red) and myosin 7a (green) in the middle turns of cochleae. (I) Quantification of the number of MitoSOX-Red-immunolabeled hair cells per 200 µm in the middle turns of cochleae. Data are shown as the mean \pm SEM. $^{****}P < 0.0001$ vs. control, $^{####}P < 0.0001$ vs. cisplatin-treated only. Cis: cisplatin; HC: hair cell; GAPDH: glyceraldehyde 3-phosphate dehydrogenase; TUNEL: TdT-mediated dUTP nick end labeling.

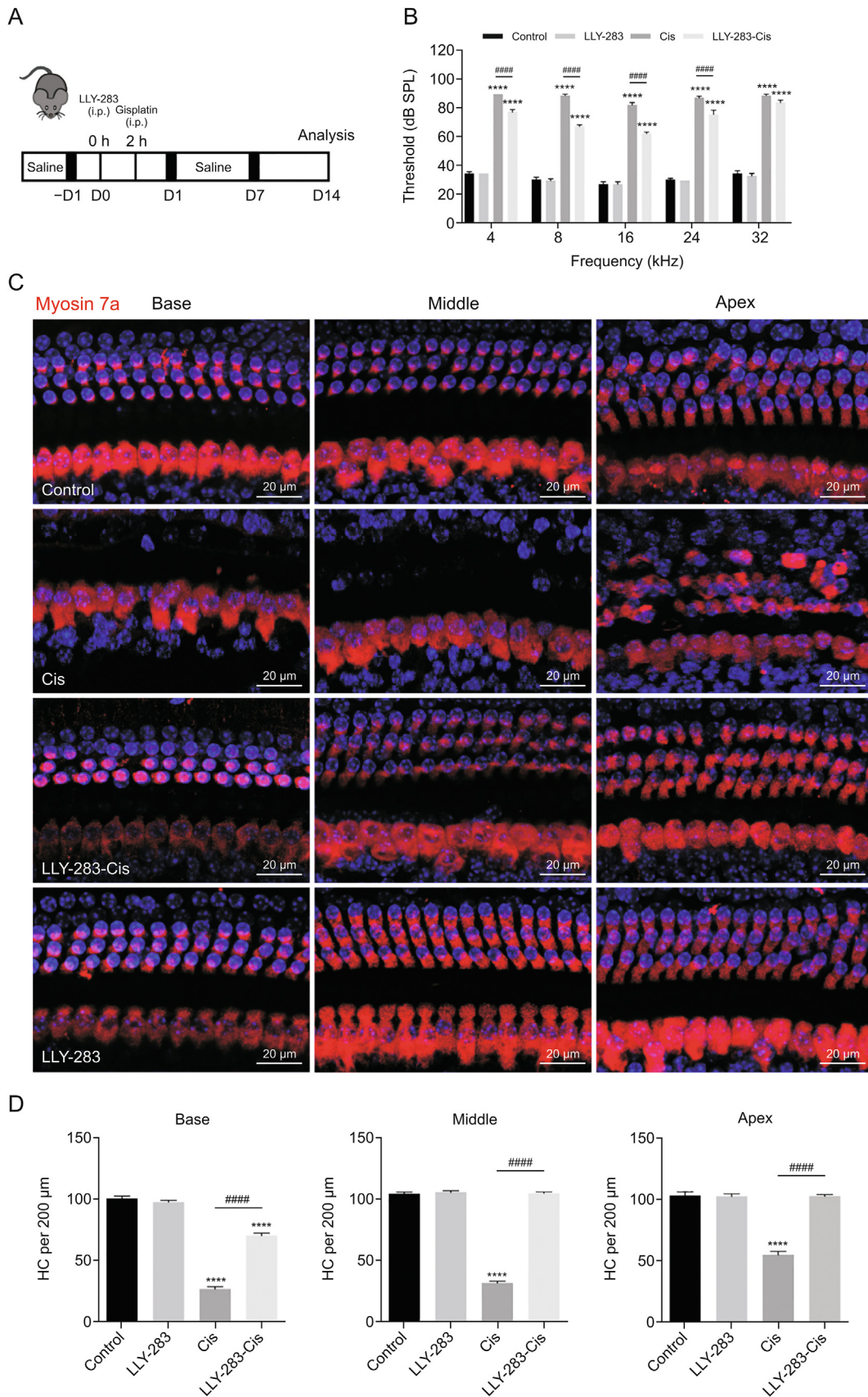


Fig. 3. LLY-283 attenuates cisplatin-induced hearing loss in vivo. (A) Experimental scheme. Mice were divided into 4 groups: control, LLY-283, cisplatin, cisplatin + LLY-283 (LLY-283-Cis). (B) Auditory brainstem response (ABR) thresholds were measured 2 day after cisplatin treatment ($n = 6$ mice per group). Data are presented as the mean \pm standard error of the mean (SEM). **** $P < 0.0001$ vs. control; ##### $P < 0.0001$ vs. cisplatin-treated only. (C) Representative images of immunostaining for myosin 7a (red) in the basal, middle, and

A NF + CtBP2 + Myosin 7a

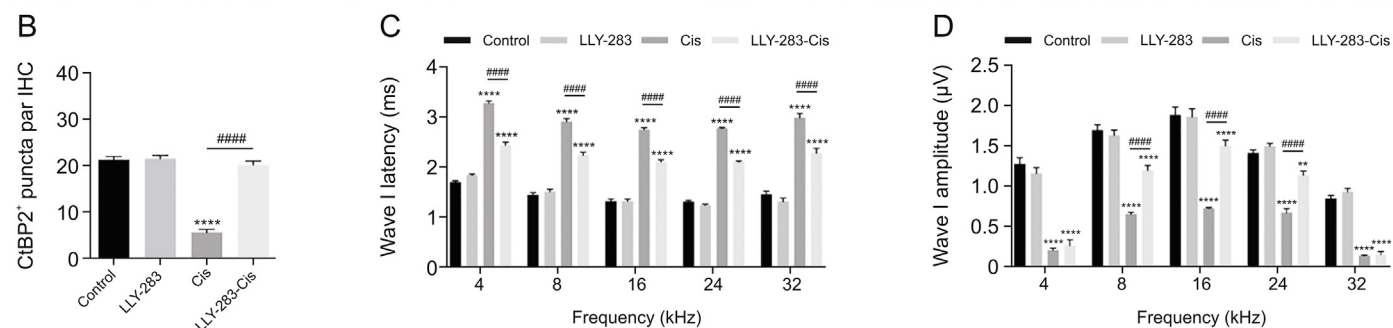
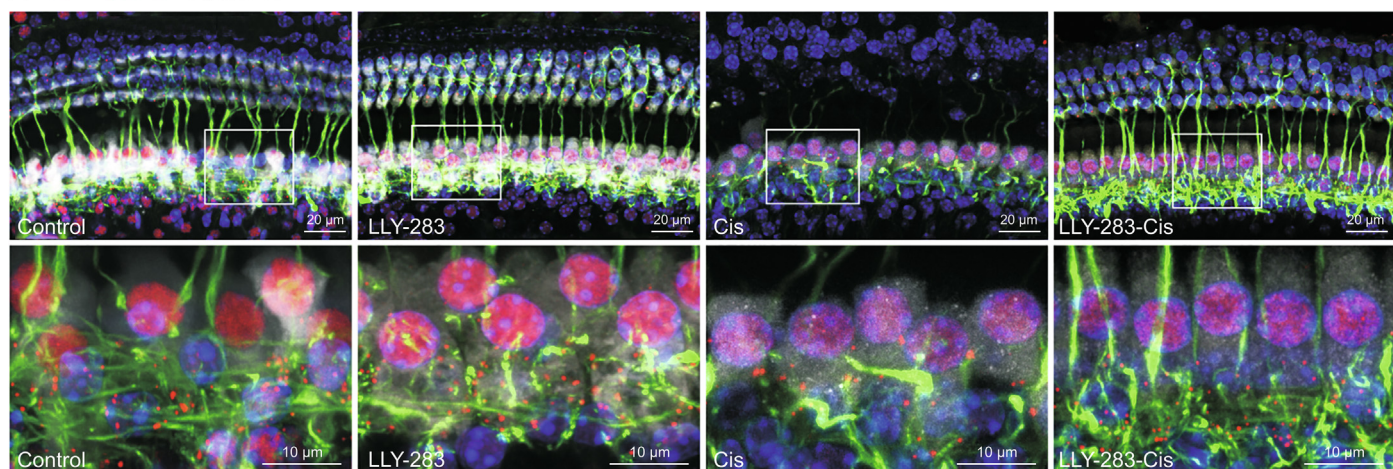


Fig. 4. LLY-283 protects mice from cisplatin-induced injury of presynaptic ribbons and afferent fibers. (A) Representative immunolabeling images of NF (green), CtBP2 (red), and myosin 7a (white) in the middle turns of cochleae from each treatment group. (B) Quantification of CtBP2-labeled presynaptic ribbons per IHC ($n = 16$ IHCs from 4 cochleae in each group). Data are presented as the mean \pm standard error of the mean (SEM). **** $P < 0.0001$ vs. control; ##### $P < 0.0001$ vs. cisplatin-treated only. (C, D) Typical Auditory brainstem response (ABR) wave I latencies (C) and amplitudes (D) of mice at testing frequencies of 4, 8, 16, 24, and 32 kHz under each experimental condition ($n = 6$ mice for each treatment). Data are presented as the mean \pm SEM. ** $P < 0.01$ and **** $P < 0.0001$ vs. control; ##### $P < 0.0001$ vs. cisplatin-treated only. Cis: cisplatin; NF: neurofilament; IHC: inner hair cell.

previously described [15]. Briefly, we administered LLY-283 (10 mg/kg) to C57 mice 2 h before cisplatin (30 mg/kg) injection, which was followed by injection of saline for 7 consecutive days (twice per day) after cisplatin stimulation (Fig. 3A). Then, we conducted an ABR test 14 day later to evaluate hearing loss. As shown in Fig. 3B, the ABR threshold shifts in response to cisplatin administration were significantly elevated at all the tested frequencies (4 kHz, 8 kHz, 16 kHz, 24 kHz, and 32 kHz) compared with those in controls. Interestingly, LLY-283 pretreatment significantly reduced these ABR threshold shifts at 4–24 kHz compared with those in the cisplatin-treated only group; however, the protective effects of LLY-283 against these threshold elevations were not apparent at 32 kHz (Fig. 3B). Furthermore, immunofluorescence staining with anti-myosin 7a antibody revealed that cisplatin induced a significant level of outer HC death compared with that in the control; however, mice pretreated with LLY-283 had no considerable loss of outer HCs (Figs. 3C and D), indicating that inhibition of PRMT5 alleviated cisplatin-induced hearing loss and HC damage. Importantly, we determined that LLY-283 administration alone did not significantly alter ABR threshold, HC morphology, or HC number.

We next aimed to evaluate the effects of LLY-283 on the cisplatin-induced loss of cochlear presynaptic ribbons and afferent fibers. We costained cochlear sections with anti-CtBP2 and anti-

neurofilament (NF) antibodies to visualize presynaptic ribbons and afferent innervations, respectively (Fig. 4A). As expected, NF staining revealed a loss of server afferent fibers in the cochleae of cisplatin-damaged mice compared with that in untreated control mice. In contrast, LLY-283 pretreatment significantly increased the number of NF-positive cochlear afferent fibers in the presence of cisplatin (Fig. 4A). Notably, we observed that after cisplatin administration, cochleae from LLY-283-pretreated mice had a significantly higher density of CtBP2-labeled presynaptic ribbons than the cisplatin-treated only group (Fig. 4B). We also detected that the counts of cochlear afferent fibers and presynaptic ribbons were similar between the control and LLY-283-treated alone mice. We then measured the mean ABR wave I latency and amplitude to assess the activity of the remaining auditory nerves. As shown in Fig. 4C, the ABR wave I latencies at all tested frequencies in cisplatin-treated mice were significantly increased compared with those in control mice; however, LLY-283 pretreatment significantly attenuated this cisplatin-induced increase. ABR wave I amplitudes are shown in Fig. 4D. We found that the ABR amplitudes in LLY-283-pretreated mice were remarkably increased compared with those in cisplatin-treated mice (Fig. 4D). Overall, LLY-283 pretreatment effectively reduced the sensitivity to cisplatin-induced losses of HCs, cochlear afferent fibers, and presynaptic ribbons.

apical turns of cochleae from the control and experimental groups. (D) Quantification of myosin 7a-immunolabeled HCs ($n = 8$ cochleae). Data are presented as the mean \pm SEM. **** $P < 0.0001$ vs. control; ##### $P < 0.0001$ vs. cisplatin-treated only. Cis: cisplatin; HC: hair cell.

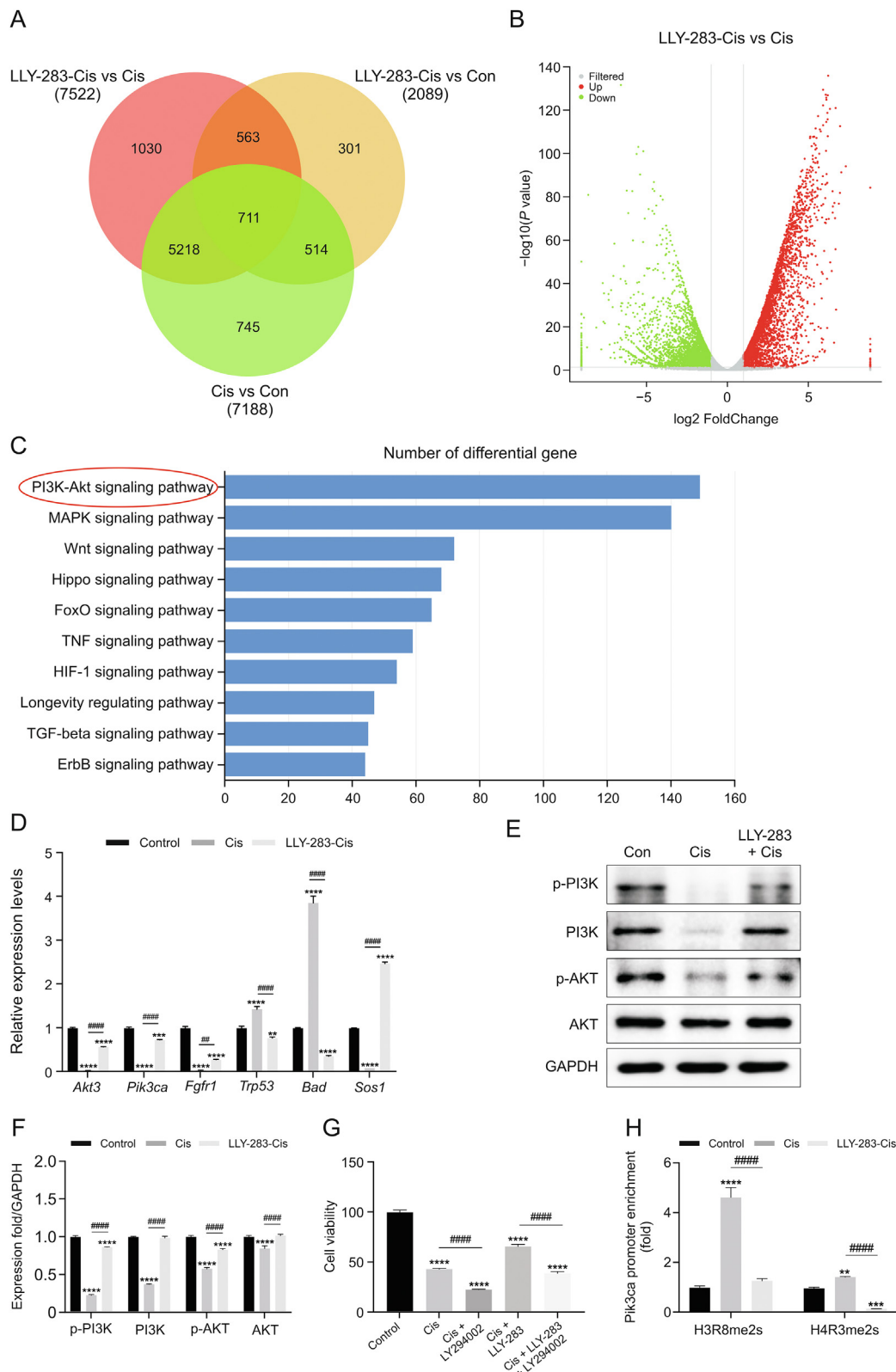


Fig. 5. RNA-seq reveals the PI3K/Akt pathway as a key regulator following PRMT5 inhibition in cisplatin-treated HEI-OC1 cells. (A) A Venn diagram depicting the number of differentially expressed genes (DEGs) between the 2 treatment groups. (B) A volcano plot representing the statistically significant DEGs from the cisplatin vs. LLY-283+cisplatin groups, as determined by RNA-seq in HEI-OC1 cells. Each gene is marked as a dot in red or green color, indicating the differentially expressed transcripts that are significantly enriched and perturbed, respectively, in LLY-283+cisplatin-treated cells. (C) Kyoto encyclopedia of genes and genomes (KEGG) enrichment analysis showing the distribution of terms exhibiting statistically significant differences. (D) The relative mRNA levels of indicated genes were normalized to the level of Gapdh, as determined by quantitative real-time reverse-transcription polymerase chain reaction (qRT-PCR). Data are expressed as the mean \pm standard error of the mean (SEM) from 3 independent experiments. ** $P < 0.01$, *** $P < 0.001$, and **** $P < 0.0001$ vs. control; # $P < 0.01$, ### $P < 0.0001$ vs. cisplatin-treated only. (E, F) Western blot analysis and histograms of the expressions of PI3K, p-PI3K, AKT, and p-AKT. Data are expressed as the mean \pm SEM of 3 independent experiments. **** $P < 0.0001$ vs. control; ##### $P < 0.0001$ vs. cisplatin-treated only. (G) The effect of PI3K inhibitor

3.4. Inhibition of PRMT5 alleviated cisplatin-induced HC apoptosis by suppressing activating PI3K/Akt pathway

To elucidate the genome-wide mechanisms underlying the protective effects of inhibiting PRMT5 on HC survival, we isolated total RNA from HEI-OC1 cells and conducted RNA sequencing. Our analysis revealed that exposure to cisplatin with or without LLY-283 pretreatment resulted in significant changes in the levels of expression of thousands of genes. We selected the differentially expressed genes (DEGs) among different groups with P -value < 0.05 and fold change ≥ 2 . As shown in Fig. 5A, we identified a total of 7522 genes as discriminatively expressed between LLY-283+cisplatin-treated and cisplatin-treated cells, including 3778 upregulated and 3744 downregulated genes. The volcano plot in Fig. 5B illustrates the gene expression patterns in cells treated with LLY-283+cisplatin. KEGG pathway analysis based on DEGs (Fig. 5C) revealed significant changes in several pathways, with those in the PI3K/Akt signaling pathway being the most prominent (Fig. 5I). To validate the changes in the mRNA levels of selected genes identified from the RNA-seq analysis (Fig. 5D), we performed quantitative real-time reverse-transcription polymerase chain reaction (qRT-PCR) analysis using primers listed in Table S1. Our results were consistent with the RNA-seq data, showing that the levels of expression of *Akt3*, *Pik3ca*, *Fgfr1*, and *Sos1* were significantly decreased in cells exposed to cisplatin compared with those in control cells; however, pretreatment with LLY-283 effectively increased the levels of expression of these genes relative to those in cells treated with cisplatin alone. Additionally, we observed that the levels of transcripts of key apoptosis-related proteins *Trp53* and *Bad* were significantly increased in cisplatin-treated cells compared with those in untreated cells; however, they were effectively decreased using LLY-283 pretreatment.

To confirm the alterations in the PI3K/Akt pathway at the posttranslational levels, we performed western blotting analysis on HEI-OC1 cells. The expression of PI3K, p-PI3K, and p-AKT was markedly downregulated in cells exposed to cisplatin compared with that in control cells; however, pretreatment with LLY-283 reversed the effect in the expression of these proteins in cisplatin-treated cells (Figs. 5E and F). Furthermore, we introduced the potent PI3K inhibitor LY294002 to examine the underlying function of PI3K in the LLY-283-mediated attenuation of ototoxicity after cisplatin treatment. Interestingly, we observed that LY294002 treatment partly abolished the antiapoptotic effects of LLY-283 in cisplatin-treated HEI-OC1 cells (Fig. 5G). These lines of evidence suggested that LLY-283 activates the PI3K/Akt signaling pathway in cisplatin-treated HEI-OC1 cells.

We also found that the mRNA levels of *Pik3ca* were significantly increased in LLY-283+cisplatin cells compared with those in cisplatin-treated only cells, as determined by RNA-Seq and qRT-PCR analysis. H4R3me2s and H3R8me2s are known to function as transcriptional repressors, while LLY-283 is known to repress these histone modifications. To investigate the effect of LLY-283 on H4R3me2s and H3R8me2s at the *Pik3ca* promoter in HEI-OC1 cells, we performed CUT&Tag-qPCR analysis. We determined that LLY-283 significantly decreased the levels of H3R8me2s and

H4R3me2s at the *Pik3ca* promoter region compared with those in cisplatin-treated only cells (Fig. 5H). These findings suggested that LLY-283 might protect HEI-OC1 cells against cisplatin-induced injury and apoptosis by upregulating the activity of PI3K/Akt through a reduction in the levels of repressive histone modifications at the promoter regions of the *Pik3ca* gene. We also confirmed the protective effect of another PRMT5 inhibitor, EPZ015666, on cisplatin-treated HCs and SGNs (Fig. 6), which was consistent with the LLY-283 data.

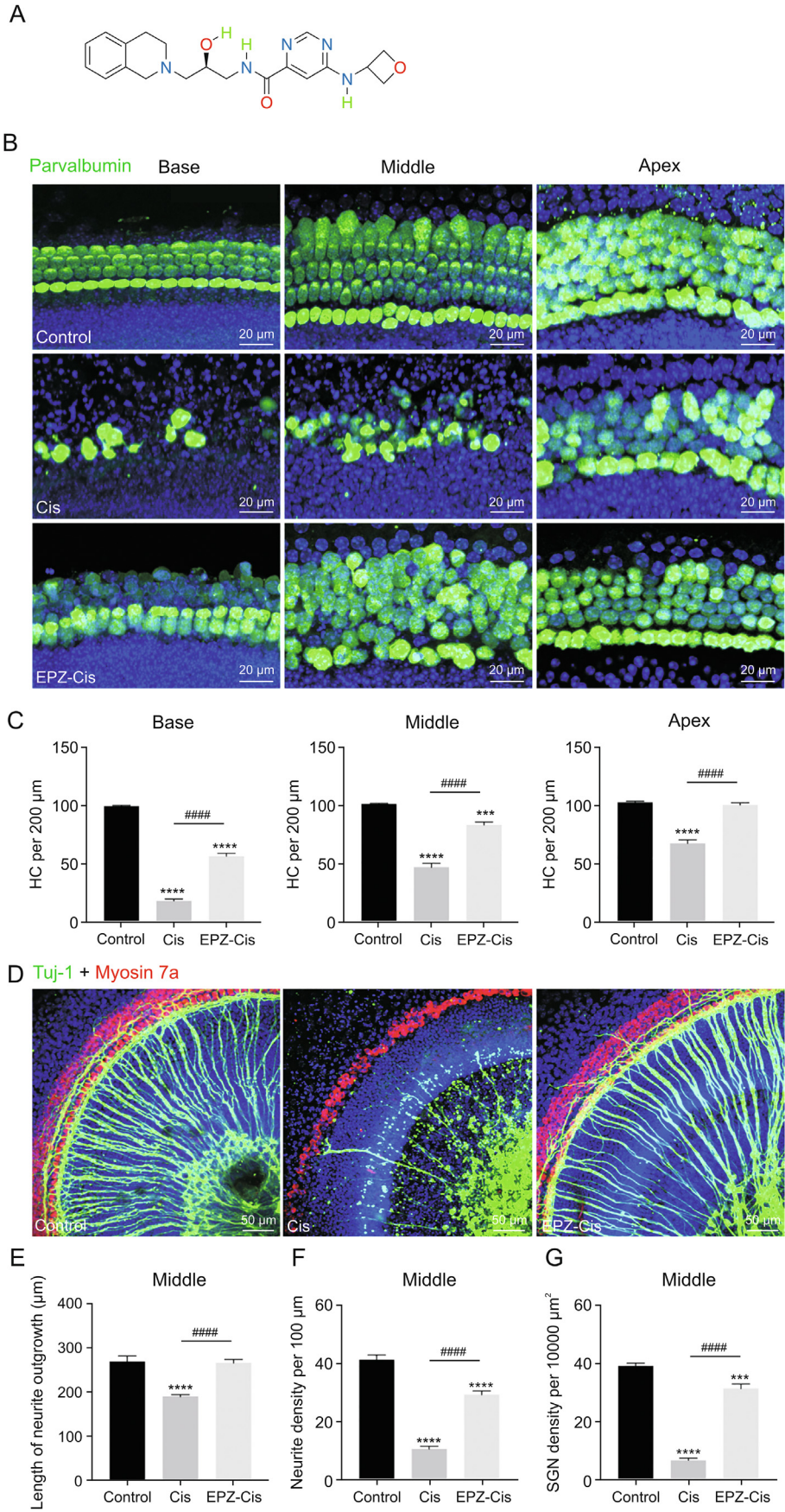
4. Discussion

Our in vitro and in vivo results demonstrated that inhibition of PRMT5 significantly reduced the extent of insult-induced ototoxicity by decreasing apoptosis and promoting the recovery of mitochondrial function. These findings highlight the requirement for further investigation into the potential clinical use of PRMT5 inhibitors for the treatment of hearing loss.

PRMT5 plays a role in regulating various biological processes, including transcription [36], RNA metabolism [37], signal transduction [38], and cellular differentiation [39]. However, the mechanisms underlying the effects of PRMT5 on these processes are not fully understood. Previous studies have shown that PRMT5 maintains the pluripotency of mouse embryonic stem cells by downregulating the expression of specific differentiation-related genes [28]. Interestingly, embryonic lethality was observed in *Prmt5*^{-/-} murine embryos, obstructing the production of embryonic stem ES cells. Likewise, PRMT5 is essential for the proliferation of human embryonic stem cells through the regulation of the expression of the cell cycle protein P57 [40]. PRMT5 also plays a role in tissue- or cell-specific differentiation processes, such as muscle, primordial germ cells, and nerve cells [17,27,39,41–43]. Dacwag et al. [39] reported that PRMT5 facilitates myogenesis through interaction with ATP-dependent chromatin remodeling complexes. Kanade et al. [43] showed that PRMT5 was involved in human keratinocyte differentiation by reducing p38 δ phosphorylation and asserting its role in p38 δ -ERK signaling. Additionally, PRMT5 and PRMT3 were shown to bind to methylate Nav1.5, a new regulator identified in cardiac pathophysiology, thus suggesting a potential role for PRMT5 in the treatment of heart disease [44].

The significant role of PRMT5 in various cellular processes, including its interaction with multiple pathways, shows that it is an attractive target for drug development and diagnostics [36]. Recently, several small molecule inhibitors targeting PRMT5 have been discovered [45–47]. However, most of these inhibitors target the SAM-binding domain, which interferes with the interaction between PRMT5 and SAM and thus are often inefficient or lack cellular or in vivo activity. Fortunately, EPZ015666, a PRMT5 inhibitor that competes with its substrate and has cellular activity, has been shown to have antiproliferative effects in both in vitro and in vivo mantle cell lymphoma models [48,49]. Its discovery has provided new clues for the development of non-SAM competitive inhibitors. Recently, a newly screened inhibitor, LLY-283, was shown to inhibit the activity of the PRMT5:MEP50 complex in vitro. Unlike EPZ015666, LLY-283 binds to and occupies the SAM pocket. Moreover, it is a low nanomolar inhibitor of the PRMT5:MEP50 complex, with higher

LY294002 on cell viability. HEI-OC1 cells were pretreated with LY294002 and LLY-283 for 2 h, and then cotreated with cisplatin for 24 h. The cell viability of each group was tested using CCK-8. Data are expressed as the mean \pm SEM. **** $P < 0.0001$ vs. control; ##### $P < 0.0001$ vs. cisplatin-treated only or LLY-283+cisplatin. (H) Cleavage under targets and tagment-quantitative polymerase chain reaction (CUT&Tag-qPCR) analyzed the enrichment of H3R8me2s and H4R3me2s on the *Pik3ca* promoter. Data are normalized to the values of IgG controls and are expressed as the mean \pm SEM of 3 independent experiments. ** $P < 0.01$, *** $P < 0.001$, and **** $P < 0.0001$ vs. control; ##### $P < 0.0001$ vs. cisplatin-treated only. Cis: cisplatin; PI3K: phosphatidylinositol 3-kinase; GAPDH: glyceraldehyde 3-phosphate dehydrogenase.



selectivity to PRMT5 than other methyltransferases [50]. This study demonstrated that the expression of PRMT5 in HCs was increased with the upregulation in the levels of H3R8me2s and H4R3me2s after treatment with cisplatin, thereby indicating PRMT5 to be a crucial target. Conversely, inhibiting the activity of PRMT5 with LLY-283 exerted strong protective effects by attenuating cisplatin-induced apoptosis. Moreover, experiments using mouse models verified the antiapoptotic effect of LLY-283 *in vivo*.

Irreversible opening of the mitochondrial permeability transition pore has been reported to induce loss of $\Delta\Psi_m$ [51], which in turn triggers the release of cytochrome c into the cytoplasm and activates the expression of Bcl2-associated X protein (Bax) and apoptosis-related proteins (including APAF-1 and caspase-3/9), thereby ultimately leading to apoptosis [52]. Consistent with these findings, our study showed that cisplatin-induced hair cell apoptosis was related to the increased levels of ROS. Treatment with LLY-283 resulted in a significant reduction in the levels of ROS in HCs compared with those in the cisplatin-treated alone group. Consistent with this study, Diao et al. [53] reported that inhibition of PRMT5 decreased the levels of proapoptotic proteins (including GSDMD-N, NLRP3, ASC, caspase-1/11, and IL-1 β) and attenuated the production of ROS *in vitro*.

To investigate the genome-wide mechanisms underlying the protective effect of inhibiting PRMT5 on hair cells, we performed RNA sequencing on HEI-OC1 cells treated with or without LLY-283 following cisplatin-induced damage. Our RNA-seq data showed changes in the levels of complex apoptosis-related pathways in HEI-OC1 cells, which is consistent with the observed decrease in the number of apoptotic cells upon PRMT5 inhibition. The PI3K/Akt pathway participates in many cellular processes, including cell cycle regulation, proliferation, apoptosis, survival, and metabolism [54]. Our RNA-seq analysis revealed that PRMT5 was involved in the regulation of the PI3K/Akt signaling in HEI-OC1 cells, providing new insights into previously reported mechanisms. For example, to exert its oncogenic functions, PRMT5 was shown to promote AKT signaling by directly methylating AKT1 at R391 [55]. In a diet-induced obesity mouse model, knockdown or enzymatic inhibition of PRMT5 increased the expression of PPAR α and levels of PGC-1 α by reducing the phosphorylation of AKT [56]. In this study, we investigated the effect of the PRMT5 inhibitor LLY-283 on the PI3K/Akt signaling in mouse HEI-OC1 cells. Our data revealed that the level of PI3K in HEI-OC1 cells exposed to cisplatin was significantly lower than that in normal control cells. However, inhibition of PRMT5 rescued the cisplatin-induced reduction in the levels of p-PI3K, PI3K, and p-AKT.

Furthermore, the PI3K inhibitor LY294002 partially blocked the antiapoptotic function of LLY-283, indicating that the PI3K/Akt pathway might play an important role in the protective effects of LLY-283 against cisplatin-generated injury in HCs. Hence, the potential relationship between PRMT5 and PI3K pathways is intriguing and warrants further investigation. Future studies need to explore the specific mechanisms by which inhibition of PRMT5

regulates the activation of PI3K and whether it can be exploited for therapeutic purposes. In addition, investigating the role of PRMT5 and PI3K pathways in other cellular processes and disease states might provide new insights and potential therapeutic approaches for a broader spectrum of disorders.

It is widely accepted that the PRMT5-catalyzed histone arginine methylation of H4R3me2s and H3R8me2s is generally associated with transcriptional repression [57], although that of H3R8 has also been linked to transcriptional activation [58]. Our study indicated that inhibiting the activity of PRMT5 reduced the expression of H4R3me2s and H3R8me2s and promoted the transcription of *Pik3ca*. However, the epigenetic role of PRMT5 on other markers cannot be ruled out. Further investigation of the role of histone arginine methylation in regulating gene expression and the antiapoptotic mechanism of PRMT5 inhibition is essential for determining the therapeutic potential of targeting PRMT5 in ototoxic injury-induced hearing loss. New models, such as cellular or mouse models of PRMT5 overexpression or deletion, will be indispensable for future investigations of the biological functions of PRMT5. Comparing the effects of inhibiting or overexpressing PRMT5 in these models might lead to a better understanding of the role of PRMT5 in cellular processes and disease states and help identify potential therapeutic targets.

Our findings collectively demonstrated that inhibiting PRMT5 had strong preventative effects on hearing deterioration. *In vitro* studies using a PRMT5 inhibitor significantly attenuated cisplatin-induced apoptosis in HCs and SGNs by reducing oxidative stress and activating the PI3K/Akt pathway. Furthermore, our proof-of-concept *in vivo* data confirmed that the PRMT5 inhibitor reduced the cisplatin-induced loss of HCs, cochlear afferent fibers, and presynaptic ribbons, indicating its potential as an effective therapeutic strategy. These findings suggested that PRMT5 inhibitors might be powerful agents for preventing cisplatin-induced hearing loss.

CRediT author statement

Zhiwei Zheng: Project administration, Methodology, Validation, Investigation, Writing - Original draft preparation; **Benyu Nan:** Project administration, Investigation, Writing - Reviewing and Editing; **Chang Liu:** Project administration, Methodology, Validation, Investigation, Writing - Original draft preparation; **Dongmei Tang:** Investigation, Software, Writing - Original draft preparation; **Wen Li:** Investigation, Formal analysis; **Liping Zhao:** Validation, Data curation; **Guohui Nie:** Conceptualization, Supervision, Resources, Project administration; **Yingzi He:** Conceptualization, Supervision, Resources, Project administration.

Declaration of competing interest

The authors declare that there are no conflicts of interest.

Fig. 6. Inhibition of PRMT5 by EPZ015666 prevents cisplatin-induced damage in HCs and SGNs *in vitro*. (A) Chemical structure of EPZ015666. (B) Immunostaining with the anti-parvalbumin antibody (green) in the basal, middle, and apical turns of cochleae after different treatments. (C) Quantification of parvalbumin-immunolabeled hair cells per 200 μm in three turns of cochleae after different treatments ($n = 7$ cochleae). Data are expressed as the mean \pm standard error of the mean (SEM). *** $P < 0.001$ and **** $P < 0.0001$ vs. control; ##### $P < 0.0001$ vs. cisplatin-treated only. (D) Representative images of immunolabeling for Tuj-1 (green) and myosin 7a (red) in the middle turns of cochleae from different treatment groups. (E–G) Quantification analysis of the length of neurite outgrowth (E), neurite densities (F), and SGN soma densities (G) from the middle turns of cochlear explants under all experimental conditions ($n = 8$ SGN explants). Data are expressed as the mean \pm SEM. *** $P < 0.001$ and **** $P < 0.0001$ vs. control; ##### $P < 0.0001$ vs. cisplatin-treated only. Cis: cisplatin; EPZ-Cis: EPZ015666 + cisplatin; HC: hair cell; SGN: spiral ganglion neuron.

Acknowledgments

This work was supported by grants from the National Natural Science Foundation of China (Grant Nos.: 82271158, 82192865, and 82071045), and Wenzhou Municipal Science and Technology Research Program (Grant No.: 2021Y0681).

Appendix A. Supplementary data

Supplementary data to this article can be found online at <https://doi.org/10.1016/j.jpha.2023.04.014>.

References

- Z.P. Stojanova, T. Kwan, N. Segil, Epigenetic regulation of Atoh1 guides hair cell development in the mammalian cochlea, *Development* 142 (2015) 3529–3536.
- D. Roellig, M.E. Bronner, The epigenetic modifier DNMT3A is necessary for proper otic placode formation, *Dev. Biol.* 411 (2016) 294–300.
- R.A. Uribe, A.L. Buzzi, M.E. Bronner, et al., Histone demethylase KDM4B regulates otic vesicle invagination via epigenetic control of Dlx3 expression, *J. Cell Biol.* 211 (2015) 815–827.
- Y.Z. He, H.Q. Yu, S. Sun, et al., Trans-2-phenylcyclopropylamine regulates zebrafish lateral line neuromast development mediated by depression of LSD1 activity, *Int. J. Dev. Biol.* 57 (2013) 365–373.
- Y.Z. He, Z.M. Wang, S.Y. Sun, et al., HDAC3 is required for posterior lateral line development in zebrafish, *Mol. Neurobiol.* 53 (2016) 5103–5117.
- Y.Z. He, D.M. Tang, W.Y. Li, et al., Histone deacetylase 1 is required for the development of the zebrafish inner ear, *Sci. Rep.* 6 (2016), 16535.
- Y. He, H. Mei, H. Yu, et al., Role of histone deacetylase activity in the developing lateral line neuromast of zebrafish larvae, *Exp. Mol. Med.* 46 (2014) e94.
- Y.Z. He, H.Q. Yu, C.F. Cai, et al., Inhibition of H3K4me2 demethylation protects auditory hair cells from neomycin-induced apoptosis, *Mol. Neurobiol.* 52 (2015) 196–205.
- K. Nimura, K. Ura, H. Shiratori, et al., A histone H3 lysine 36 trimethyltransferase links Nkx2-5 to Wolf-Hirschhorn syndrome, *Nature* 460 (2009) 287–291.
- M. Ahmed, K. Ura, A. Streit, Auditory hair cell defects as potential cause for sensorineural deafness in Wolf-Hirschhorn syndrome, *Dis. Models Mech.* 8 (2015) 1027–1035.
- T. Kouzarides, Chromatin modifications and their function, *Cell* 128 (2007) 693–705.
- P.A. Jones, Functions of DNA methylation: islands, start sites, gene bodies and beyond, *Nat. Rev. Genet.* 13 (2012) 484–492.
- B.N. Zheng, C.H. Ding, S.J. Chen, et al., Targeting PRMT5 activity inhibits the malignancy of hepatocellular carcinoma by promoting the transcription of HNF4 α , *Theranostics* 9 (2019) 2606–2617.
- R.S. Blanc, S. Richard, Arginine methylation: the coming of age, *Mol. Cell* 65 (2017) 8–24.
- Y.Z. He, W. Li, Z.W. Zheng, et al., Inhibition of Protein arginine methyltransferase 6 reduces reactive oxygen species production and attenuates aminoglycoside- and cisplatin-induced hair cell death, *Theranostics* 10 (2020) 133–150.
- N. Stopa, J.E. Krebs, D. Shechter, The PRMT5 arginine methyltransferase: many roles in development, cancer and beyond, *Cell, Mol. Life Sci.* 72 (2015) 2041–2059.
- V. Karkhanis, Y.J. Hu, R.A. Baiocchi, et al., Versatility of PRMT5-induced methylation in growth control and development, *Trends Biochem. Sci.* 36 (2011) 633–641.
- E.C. Cho, S.S. Zheng, S. Munro, et al., Arginine methylation controls growth regulation by E2F-1, *EMBO J.* 31 (2012) 1785–1797.
- M. Kanda, D. Shimizu, T. Fujii, et al., Protein arginine methyltransferase 5 is associated with malignant phenotype and peritoneal metastasis in gastric cancer, *Int. J. Oncol.* 49 (2016) 1195–1202.
- J.Q. Ren, Y.Q. Wang, Y.H. Liang, et al., Methylation of ribosomal protein S10 by protein-arginine methyltransferase 5 regulates ribosome biogenesis, *J. Biol. Chem.* 285 (2010) 12695–12705.
- S.E. LeBlanc, Q. Wu, P. Lamba, et al., Promoter-enhancer looping at the PPAR γ 2 locus during adipogenic differentiation requires the Prmt5 methyltransferase, *Nucleic Acids Res.* 44 (2016) 5133–5147.
- S. Majumder, L. Alinari, S. Roy, et al., Methylation of histone H3 and H4 by PRMT5 regulates ribosomal RNA gene transcription, *J. Cell. Biochem.* 109 (2010) 553–563.
- E. Fabbri, S. El Messaoudi, J. Polanowska, et al., Negative regulation of transcription by the type II arginine methyltransferase PRMT5, *EMBO Rep.* 3 (2002) 641–645.
- Y.L. Jin, J.F. Zhou, F. Xu, et al., Targeting methyltransferase PRMT5 eliminates leukemia stem cells in chronic myelogenous leukemia, *J. Clin. Invest.* 126 (2016) 3961–3980.
- S. Huang, Y.Y. Chi, Y. Qin, et al., CAPG enhances breast cancer metastasis by competing with PRMT5 to modulate STC-1 transcription, *Theranostics* 8 (2018) 2549–2564.
- J. Serio, J. Ropa, W. Chen, et al., The PAF complex regulation of Prmt5 facilitates the progression and maintenance of MLL fusion leukemia, *Oncogene* 37 (2018) 450–460.
- A. Chittka, J. Nitarska, U. Grazini, et al., Transcription factor positive regulatory domain 4 (PRDM4) recruits protein arginine methyltransferase 5 (PRMT5) to mediate histone arginine methylation and control neural stem cell proliferation and differentiation, *J. Biol. Chem.* 287 (2012) 42995–43006.
- W.W. Tee, M. Pardo, T.W. Theunissen, et al., Prmt5 is essential for early mouse development and acts in the cytoplasm to maintain ES cell pluripotency, *Genes Dev.* 24 (2010) 2772–2777.
- F. Liu, G.Y. Cheng, P.J. Hamard, et al., Arginine methyltransferase PRMT5 is essential for sustaining normal adult hematopoiesis, *J. Clin. Invest.* 125 (2015) 3532–3544.
- H. Tanaka, Y. Hoshikawa, T. Oh-hara, et al., PRMT5, a novel TRAIL receptor-binding protein, inhibits TRAIL-induced apoptosis via nuclear factor- κ B activation, *Mol. Cancer Res.* 7 (2009) 557–569.
- H. Wei, B. Wang, M. Miyagi, et al., PRMT5 dimethylates R30 of the p65 subunit to activate NF- κ B, *Proc. Natl. Acad. Sci. USA* 110 (2013) 13516–13521.
- S.K. Lim, Y.W. Jeong, D.I. Kim, et al., Activation of PRMT1 and PRMT5 mediates hypoxia- and ischemia-induced apoptosis in human lung epithelial cells and the lung of miniature pigs: the role of p38 and JNK mitogen-activated protein kinases, *Biochem. Biophys. Res. Commun.* 440 (2013) 707–713.
- M.C. Braun, C.N. Kelly, A.E. Prada, et al., Human PRMT5 expression is enhanced during *in vitro* tubule formation and after *in vivo* ischemic injury in renal epithelial cells, *Am. J. Nephrol.* 24 (2004) 250–257.
- H. Yu, Q. Lin, Y. Wang, et al., Inhibition of H3K9 methyltransferases G9a/GLP prevents ototoxicity and ongoing hair cell death, *Cell Death Dis.* 4 (2013) e506.
- H.S. Kaya-Okur, S.J. Wu, C.A. Codomo, et al., CUT&Tag for efficient epigenomic profiling of small samples and single cells, *Nat. Commun.* 10 (2019) 1930.
- H. Chen, B. Lorton, V. Gupta, et al., A TGF β -PRMT5-MEP50 axis regulates cancer cell invasion through histone H3 and H4 arginine methylation coupled transcriptional activation and repression, *Oncogene* 36 (2017) 373–386.
- M. Bezzi, S.X. Teo, J. Muller, et al., Regulation of constitutive and alternative splicing by PRMT5 reveals a role for *Mdm4* pre-mRNA in sensing defects in the spliceosomal machinery, *Genes Dev.* 27 (2013) 1903–1916.
- M. Jansson, S.T. Durant, E.C. Cho, et al., Arginine methylation regulates the p53 response, *Nat. Cell Biol.* 10 (2008) 1431–1439.
- C.S. Dacwag, Y. Ohkawa, S. Pal, et al., The protein arginine methyltransferase Prmt5 is required for myogenesis because it facilitates ATP-dependent chromatin remodeling, *Mol. Cell Biol.* 27 (2007) 384–394.
- S. Gkoutela, Z.W. Li, C.J. Chin, et al., PRMT5 is required for human embryonic stem cell proliferation but not pluripotency, *Stem Cell Rev. Rep.* 10 (2014) 230–239.
- C.S. Dacwag, M.T. Bedford, S. Sif, et al., Distinct protein arginine methyltransferases promote ATP-dependent chromatin remodeling function at different stages of skeletal muscle differentiation, *Mol. Cell Biol.* 29 (2009) 1909–1921.
- C. Paul, C. Sardet, E. Fabbri, The histone- and PRMT5-associated protein COPR5 is required for myogenic differentiation, *Cell Death Differ.* 19 (2012) 900–908.
- S.R. Kanade, R.L. Eckert, Protein arginine methyltransferase 5 (PRMT5) signaling suppresses protein kinase C Δ - and p38 Δ -dependent signaling and keratinocyte differentiation, *J. Biol. Chem.* 287 (2012) 7313–7323.
- P. Beltran-Alvarez, A. Espejo, R. Schmauder, et al., Protein arginine methyltransferases-3 and-5 increase cell surface expression of cardiac sodium channel, *FEBS Lett.* 587 (2013) 3159–3165.
- H.U. Kaniskan, J. Jin, Recent progress in developing selective inhibitors of protein methyltransferases, *Curr. Opin. Chem. Biol.* 39 (2017) 100–108.
- H. Hu, K. Qian, M.C. Ho, et al., Small molecule inhibitors of protein arginine methyltransferases, *Expert Opin. Invest. Drugs* 25 (2016) 335–358.
- R. Mao, J. Shao, K. Zhu, et al., Potent, selective, and cell active protein arginine methyltransferase 5 (PRMT5) inhibitor developed by structure-based virtual screening and hit optimization, *J. Med. Chem.* 60 (2017) 6289–6304.
- E. Chan-Penebre, K.G. Kuplast, C.R. Majer, et al., A selective inhibitor of PRMT5 with *in vivo* and *in vitro* potency in MCL models, *Nat. Chem. Biol.* 11 (2015) 432–437.
- K.W. Duncan, N. Rioux, P.A. Boriack-Sjodin, et al., Structure and property guided design in the identification of PRMT5 tool compound EPZ015666, *ACS Med. Chem. Lett.* 7 (2016) 162–166.
- Z.Q. Bonday, G.S. Cortez, M.J. Grogan, et al., LLY-283, a potent and selective inhibitor of arginine methyltransferase 5, PRMT5, with antitumor activity, *ACS Med. Chem. Lett.* 9 (2018) 612–617.

- [51] Y. Tsujimoto, S. Shimizu, Role of the mitochondrial membrane permeability transition in cell death, *Apoptosis* 12 (2007) 835–840.
- [52] M. Hüttemann, S. Helling, T.H. Sanderson, et al., Regulation of mitochondrial respiration and apoptosis through cell signaling: cytochrome c oxidase and cytochrome c in ischemia/reperfusion injury and inflammation, *Biochim. Biophys. Acta* 1817 (2012) 598–609.
- [53] C. Diao, Z. Chen, T. Qiu, et al., Inhibition of PRMT5 attenuates oxidative stress-induced pyroptosis via activation of the Nrf2/HO-1 signal pathway in a mouse model of renal ischemia-reperfusion injury, *Oxid. Med. Cell. Longev.* (2019) 1–18.
- [54] B.D. Manning, A. Toker, AKT/PKB signaling: navigating the network, *Cell* 169 (2017) 381–405.
- [55] S. Yin, L. Liu, C. Brobbey, et al., PRMT5-mediated arginine methylation activates AKT kinase to govern tumorigenesis, *Nat. Commun.* 12 (2021) 3444.
- [56] L. Huang, J. Liu, X.O. Zhang, et al., Inhibition of protein arginine methyltransferase 5 enhances hepatic mitochondrial biogenesis, *J. Biol. Chem.* 293 (2018) 10884–10894.
- [57] X.J. Xu, S. Hoang, M.W. Mayo, et al., Application of machine learning methods to histone methylation ChIP-Seq data reveals H4R3me2 globally represses gene expression, *BMC Bioinf.* 11 (2010).
- [58] S. Pal, R.A. Baiocchi, J.C. Byrd, et al., Low levels of miR-92b/96 induce PRMT5 translation and H3R8/H4R3 methylation in mantle cell lymphoma, *EMBO J.* 26 (2007) 3558–3569.